Received: 3 April 2022 | Revised: 7 July 2022 | Accepted: 23 July 2022

DOI: 10.1002/suco.202200319

ARTICLE

fib CEB-FIP WILEY

Modeling statically indeterminate reinforced concrete slabs and beams under fire conditions

Patrick Bischof[1] | **Urias Morf**[1] | **Patrick Bamonte**[2] | **Walter Kaufmann**[1]

[1]Institute of Structural Engineering, Department of Civil, Environmental and Geomatic Engineering, ETH Zurich, Zurich, Switzerland

[2]Department of Civil and Environmental Engineering (DICA), Politecnico di Milano, Milan, Italy

Correspondence
Patrick Bischof, Institute of Structural Engineering, Department of Civil, Environmental and Geomatic Engineering, ETH Zurich, Zurich, Switzerland.
Email: bischof@ibk.baug.ethz.ch

Abstract

EN 1992-1-2 generally limits the redistribution of bending moments from the intermediate supports to the span for continuous reinforced concrete slabs and beams in fire conditions to 15%. While higher redistributions are allowed if sufficient rotation capacity is provided, EN 1992-1-2 does not indicate how to assess the rotation capacity. However, plastic hinges caused by the rotation demand under fire conditions are highly relevant when predicting the global response and structural safety of a structure (partially) exposed to fire. Rotation capacity is specifically necessary at support regions subjected to negative bending and fire, where concrete in compression undergoes thermal degradation while the tension chord remains close to ambient temperature. This article presents a comprehensive model for the behavior of statically indeterminate members in fire conditions, enabling to estimate whether sufficient rotation capacity is provided. Material properties specified by EN 1992-1-2 are applied combined with complementary considerations concerning (i) the biaxial compressive strength of concrete, (ii) strain hardening and limitations of the ultimate strain of reinforcement, as well as (iii) tension stiffening. Tension stiffening detrimentally influences the ductility of the tension chord, limiting the rotation capacity. When comparing predictions obtained by the model to experimental results given in the literature, the correlation is good for the investigated one-way continuous slabs and beams. However, considerable uncertainty exists regarding the type of concrete aggregate used. Moreover, uncertainties concerning the behavior of concrete under compression and fire conditions are highly relevant for modeling the region of supports with rotational restraint.

1 | INTRODUCTION

In statically indeterminate systems, temperature differences within the cross-section entail indirect actions whose magnitude depends on the predominant temperature gradient, the static system, and the member stiffness.

Discussion on this paper must be submitted within two months of the print publication. The discussion will then be published in print, along with the authors' closure, if any, approximately nine months after the print publication.

When exposed to fire, slabs experience temperature differences of several hundreds degree Celsius between the exposed and the unexposed surface, causing high restraint moments and a considerable rotation demand to redistribute these bending moments already at very low fire durations. As an example, yielding of the reinforcement above the intermediate supports initiated after merely 10–20 min under standard fire exposure in all continuous slabs tested by Kordina and Wesche.[1] The possible redistribution of bending moments depends on a member's rotation capacity, that is the inelastic rotation in the governing plastic hinge(s) from the onset of yielding to failure, which may be triggered by reinforcement rupture or concrete crushing. Rotation capacity is specifically necessary at intermediate supports, where the concrete in compression undergoes thermal degradation while the tension chord remains close to ambient temperature. Note that plastic rotations occurring in continuous members under fire conditions may by far exceed those expected at ambient temperature.

When using tabulated design data, EN 1992-1-2[2] generally limits the redistribution of bending moments caused by static loading at ambient temperature from the intermediate supports to the span in continuous reinforced concrete members under fire conditions to 15%. While higher redistributions are allowed if sufficient rotation capacity is provided, EN 1992-1-2 does not indicate how to assess it. Hence, finite element analyses are generally employed to study the behavior of statically indeterminate structures. However, such calculations are not straightforward since (i) rotation demand and rotation capacity cannot be considered separately (as often done at ambient temperature) and (ii) the easy-to-use constitutive model for reinforcing steel from EN 1992-1-2 cannot capture the actual behavior beyond yielding of the tension chord, because of the absence of the hardening branch.

The realistic modeling of plastic hinges caused by the high restraint moments under fire conditions and their corresponding large rotations is relevant for reliably predicting the global response and the structural safety of a statically indeterminate structure (partially) exposed to fire. Furthermore, such predictions are essential (i) to understand and evaluate the corresponding detailing rules given in EN 1992-1-2 and (ii) to allow a realistic evaluation of the shear forces at intermediate supports. Regarding the latter, ignoring the thermal behavior may lead to insufficient shear (punching) resistance in regions less critical in this respect at ambient temperature[3]; note that EN 1992-1-2 asks for an increased minimum thickness in the region of intermediate supports for continuous beams to prevent such issues. Furthermore, the understanding of statically indeterminate systems in the support regions is essential to account for other phenomena depending on acting compressive stresses and strains, such as explosive spalling, for example, in precast elements with thin webs.

In this study, a comprehensive model is elaborated to assess (i) the rotation demand and rotation capacity and hence, the fire resistance of statically indeterminate members as well as (ii) the material and design properties necessary for understanding the behavior of these members under fire conditions. The model builds on the Tension Chord Model (TCM),[4] which was developed by Sigrist[5] to study the rotation capacity of members subjected to bending at ambient temperature. Being based on fundamental mechanical principles, the TCM enables expressing the load-deformation behavior of reinforced concrete tension chord elements, that are parts of a member loaded in tension between two adjacent cracks, in a closed analytical form: by adopting a stepped, rigid-perfectly plastic bond shear stress-slip relationship, independent of the local bond slip, the relevant structural implications of bond—tension stiffening causing higher stiffness and reduced ductility of a tension chord—are captured without having to solve the differential equation of bond. The TCM has been implemented in several finite element models to describe the load-deformation behavior and the ultimate limit state of structural concrete members at ambient conditions, for example, Kaufmann et al.[6] However, it has not been applied to fire design to date to the authors' knowledge.

The model presented in this article describes the fire behavior of statically indeterminate reinforced concrete members subjected to uniaxial bending and exposed to fire. In a first step, the cross-sectional moment-curvature relationships for every considered time are determined. The total cross-sectional curvatures are determined by considering the thermal expansion and stress-related strains. They are based on constitutive material properties given by EN 1992-1-2 and some complementary considerations concerning the biaxial compressive strength of concrete and strain hardening of reinforcement. In a second step, the structural system is analyzed using these cross-sectional moment-curvature relationships, ensuring global equilibrium and compatibility. The implementation of the model considers one-way continuous slabs and is validated by comparing predictions to relevant experimental results from full-scale statically one-way indeterminate members under standard fire exposure.[1,7–9] In a further study, Bischof et al.[10] carried out a sensitivity study using the model presented in this article to (i) identify the most influential properties in terms of the structural behavior of statically indeterminate systems under fire conditions and (ii) generally discuss the design limit of 15% for redistributing bending moments and detailing rules given in EN 1992-1-2.

2 | THERMAL AND MECHANICAL MATERIAL PROPERTIES UNDER FIRE CONDITIONS

EN 1992-1-2 provides values and reduction coefficients for thermal material properties: the thermal emissivity, the thermal conductivity, the specific heat, and the concrete density. Furthermore, it provides values and reduction coefficients for temperature-dependent mechanical material properties: (i) the coefficients of thermal expansion for concrete $\varepsilon_{cth}(\theta_c)$ with siliceous or calcareous aggregates, as well as for reinforcing steel $\varepsilon_{sth}(\theta_s)$, (ii) stress–strain relationships for concrete in compression and for reinforcing and prestressing steel in tension or compression, and (iii) a simple linear relationship for the decay of the concrete tensile strength.

The material properties defined in EN 1992-1-2 are generally well-established and provide a good balance between ease-of-use and accuracy in describing the material behavior for structural analysis under fire conditions, which is subject to more scatter than at ambient temperature. This study considers material properties defined in EN 1992-1-2 as input data. In addition, (i) the concrete compressive strength under a biaxial stress state is discussed, (ii) the stress–strain relationship for reinforcement at elevated temperatures is complemented by considering strain-hardening and realistic ultimate strains, and (iii) the bond strength under fire conditions is explicitly introduced in a simplified manner. The material properties are used to model tension stiffening based on the TCM. The adopted complementary mechanical properties, all essential for assessing the fire behavior of statically indeterminate members but not specified by EN 1992-1-2, are discussed in the following subsections.

2.1 | Concrete compressive strength

The temperature-dependent stress–strain relationship of concrete in compression given in EN 1992-1-2 implicitly includes effects from creep and transient state strains during heating. Hence, it describes the load–displacement behavior of uniaxially loaded concrete in the built condition of a structure. EN 1992-1-2 does not explicitly define the post-peak softening behavior between the strain at maximum stress $\varepsilon_{c1,\theta}$ and the ultimate strain $\varepsilon_{cu1,\theta}$. Generally, a linear or cubic softening behavior may be adopted. In this article, a linear softening behavior is assumed. Note that post-peak softening is related to strain localization, just as at ambient temperature. Hence, the size of the fracture process zone needs to be accounted for when defining stress–strain relationships in this range, which is generally associated with high uncertainty.

EN 1992-1-2 does not provide a relationship for the ratio between uniaxial and multiaxial compressive strength. However, as can be seen from tests summarized by Lo Monte et al.,[11] the relative strength increase in biaxial compression appears to be more pronounced at elevated temperatures despite being characterized by considerable scatter. Where applicable in this study, the beneficial effect of a biaxial stress state is thus considered in a simplified manner by increasing the concrete strength at relevant positions by a factor of 1.5.

2.2 | Reinforcing steel

Figure 1 shows the temperature-dependent stress–strain relationship of reinforcing steel from EN 1992-1-2 with a thin dashed line. The relationship describes heated reinforcing steel by the slope of the linear elastic range $E_{s,\theta}$, the proportional limit $f_{sp,\theta}$, the maximum stress level $f_{sy,\theta}$, and the strain $\varepsilon_{sy,\theta}$ where the latter is first attained. Different reduction values are available for reinforcing steel depending on the class (Class N or Class X) and the type of production process ("cold worked" and "hot rolled" for Class N).

The stress–strain relationship provided in EN 1992-1-2, capturing the complete transient performance and valid for all temperatures during a fire, simplifies the actual behavior for ease-of-use but does not provide temperature-dependent information on strain hardening of the reinforcement. However, strain hardening is a prerequisite for rotation capacity. Furthermore, the stress–strain relationship defines relatively high values of the ultimate strain with $\varepsilon_{st,\theta} = 0.05$ for B500A and $\varepsilon_{st,\theta} = 0.15$ for B500B and B500C, regardless of the actual temperature. As shown in several experimental studies,[12–15] the ultimate strain of modern reinforcing steel is rather equivalent or, in some cases, even reduced compared to ambient temperature

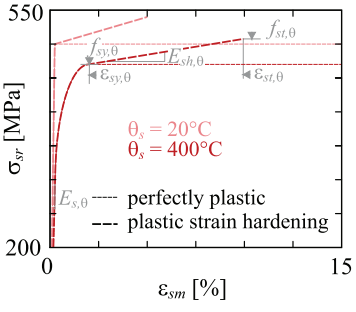

FIGURE 1 Stress-strain relationship of a bare B500B reinforcing steel at 20°C and 400°C assuming either a perfectly plastic behavior according to EN 1992-1-2 (thin dashed line) or a plastic strain hardening behavior after reaching the maximum stress level (bold dashed line, adopted for modeling in this study).

conditions in the range between 100°C and 400°C, which is relevant for the top reinforcement at intermediate supports of continuous members when exposed to fire at the bottom.

As experimental studies on the ultimate strain under fire conditions have not received sufficient attention in the fire research community, no generally agreed recommendations are currently available. In this study, strain hardening is introduced for fire conditions by scaling the hardening branch at ambient temperature, as illustrated by the bold dashed curve in Figure 1. First, the strain hardening modulus is defined by a realistic tensile strength and corresponding maximum strain at ambient temperature for reinforcing steel according to the information given in test reports[1–9] or in EN 1992-1-1.[16] Second, temperature degradation of the strain hardening modulus is assumed equivalent to that of the Young's modulus with $E_{sh,\theta}/E_{sh} = E_{s,\theta}/E_s$ (ratio of strain hardening and Young's moduli, respectively, at high temperature and ambient temperature, respectively). Furthermore, the ultimate tensile strength of the reinforcement under fire conditions $f_{st,\theta}$ is assumed to decrease proportionally to the decrease of $f_{sy,\theta}$ with $f_{st,\theta}/f_t = f_{sy,\theta}/f_y$. As a consequence, the ultimate strain is defined as

$$\varepsilon_{st,\theta} = \frac{f_{st,\theta} - f_{sy,\theta}}{E_{sh,\theta}} + \varepsilon_{sy,\theta}. \quad (1)$$

In the case of a bare B500B reinforcing bar (bold dashed curves in Figure 1), this assumption leads to ultimate strains of $\varepsilon_{st,\theta} = 0.05$ at 20°C (as defined by EN 1992-1-1) and $\varepsilon_{st,\theta} = 0.1$ at 400°C. Hence, the ultimate strain always stays clearly below the limit specified by EN 1992-1-2, particularly in the range of realistic temperatures for the top reinforcement at intermediate supports.

2.3 | Bond strength

Bond between concrete and reinforcing bars is essential for a proper anchorage of reinforcing bars and relevant for the behavior of tension chords: tension stiffening causes a higher stiffness and reduced ductility. Only if bond is suitably modeled, (i) the stiffness of reinforced concrete members may be estimated realistically and (ii) stresses and strains in concrete and steel can be modeled along an entire tension chord, both at the cracks as well as between cracks.

Sigrist[5] proposed a simplified stepped, rigid-perfectly plastic bond stress-slip relationship (assuming a constant bond strength of $\tau_{b0} = 0.6\, f_c^{2/3} = 2\, f_{ctm}$ before yielding and $\tau_{b1} = 0.3\, f_c^{2/3} = f_{ctm}$ beyond, with f_c = mean compressive strength of concrete and f_{ctm} = mean tensile strength of concrete). While more refined bond stress-slip relationships are available, they merely presume a higher level of accuracy in most cases, as (i) they equally simplify the complex phenomenon of bond (e.g., local interlocking at ribs) by assuming nominal shear stresses uniformly distributed along a nominal reinforcing bar circumference; (ii) they are calibrated using average bond stresses over a limited embedment length in tests that often fail by splitting; and (iii) the behavior is in any case subject to large uncertainty due to the scatter of material properties and, in particular, the inherent uncertainty of a factor of two in the crack spacing: at the center between two cracks with maximum spacing, f_{ctm} is reached and hence, a new crack may form or not. EN 1992-1-2 gives no specific recommendations on the nominal bond strength at elevated temperatures. Experimental results on the residual bond strength measured in standard pull-out specimens collected by Bošnjak et al.[17] indicate a considerable scatter of the temperature-dependent degradation in the range between the tensile and compressive strength degradation of concrete under fire conditions according to EN 1992-1-2.

Just like originally proposed by Sigrist[5] at ambient temperature, a stepped, rigid-perfectly plastic bond shear stress–slip relationship is assumed in this study also for elevated temperatures. The bond strength is equally assumed to be dependent on the strain of the reinforcement: In the linear elastic phase, $\tau_{b0,\theta} = 0.6\ k_{c,\theta}\ f_c^{2/3}$ is applied while $\tau_{b1,\theta} = 0.3\ k_{c,\theta}\ f_c^{2/3}$ is generally assumed beyond the proportional limit ($f_{sp,\theta}/E_{s,\theta}$). The thermal degradation of the bond strength is thus assumed to be equivalent to the thermal degradation of the concrete compressive strength $k_{c,\theta}$ according to EN 1992-1-2. Note that for continuous members, the bond strength is primarily relevant for modeling the tension chord at intermediate supports, with temperature ranges generally below 200°C (which is why the assumption on the thermal degradation is of secondary importance for this region). The bond shear stress-slip relationship is assumed to be valid for all types of passive reinforcement (bars and meshes, disregarding welded transverse reinforcement).

3 | STATICALLY INDETERMINATE REINFORCED CONCRETE BEAMS AND SLABS UNDER FIRE CONDITIONS

The moment-curvature relationships of the relevant cross-sections under fire conditions are determined using the material properties from EN 1992-1-2, the complementary specifications outlined above and the TCM to account for tension stiffening. The structural system, subjected to fire and static loads, is analyzed for a specific fire duration by integrating these cross-sectional

moment-curvature relationships. In this study, an initially stress-free system cast at once is assumed. Neither restraint at ambient temperature nor construction stages are considered. Furthermore, as common at ambient temperature, shear strains are neglected. This assumption seems to be valid for slabs. However, it involves some uncertainties for beams with shear cracks.[7,8] The procedure outlined is similar to that applied by Dwaikat and Kodur,[18] but with the material properties discussed in Section 2 and with iterating the restraint forces and moments at the considered fire duration.

3.1 | Thermal field

The thermal field is crucial for determining the temperature-dependent material properties and, in the case of statically indeterminate systems, restraint actions. In this study, the thermal field is estimated with transient heat transfer analyses based on the following assumptions:

- the reference concrete density at 20°C is assumed to be 2300 kg/m^3 (unless known for a specific test),
- the density varies with temperature according to EN 1992-1-2,
- the specific heat of concrete corresponds to the values according to EN 1992-1-2,
- the moisture content coincides with the values given for the considered tests,
- the thermal conductivity of concrete is defined by the mixed curve proposed by Zehfuß et al.,[19] which is the curve currently proposed for the future revision of the EN 1992-1-2,
- the emissivity related to the concrete surface is assumed to be 0.7,
- the convection factor is assumed to be 25 W/(m^{2}K) and
- the reinforcement is disregarded in the thermal analyses.

A one-dimensional analysis is carried out for slabs, and a two-dimensional analysis is carried out for beams. In Figure 2, the calculated temperatures (solid lines) are compared to the ones measured (dashed lines): (a) and (b) in Slab KW-2 of the test series by Kordina and Wesche[1] and (c) in Beam W-5 of the test series by Wesche.[8] Note that the specimens are denominated according to the author names here, for example, KW-9 for Slab 9 from Kordina and Wesche[1] or W-1 for Beam 1 from Wesche.[8] The calculated values are in reasonably good agreement with the measured temperatures, with higher precision for the slabs than for the beams.

3.2 | Tension stiffening effects in members subjected to bending

As previously explained, the model applied in this study adopts the TCM, whose simple bond stress–slip relationship allows efficiently capturing the relevant structural implications of bond. It allows determining the minimum and maximum crack spacing as well as average stresses and strains in a tension chord in closed form by relating them to equilibrium formulated at the cracks.

The inherent uncertainty of whether a crack is formed in the center of a tension chord element is considered in the TCM by the factor λ, where λ = 1.0 leads to the maximum and λ = 0.5 to the minimum crack spacing, respectively. According to Kaufmann et al.,[6] and following recommendations based on bending and tension tests carried out by several researchers[20–23] the average crack spacing is assumed here as 2/3 of the maximum crack spacing (λ = 0.67). At low load levels, the TCM is used in the refined formulation proposed by Seelhofer[24] by essentially assuming a pull-out behavior until full activation of a tension chord element.

When considering a member subjected to bending (see Figures 3a and b), a virtual tension chord (qualitatively dark gray hatched in Figure 3b) with an equivalent

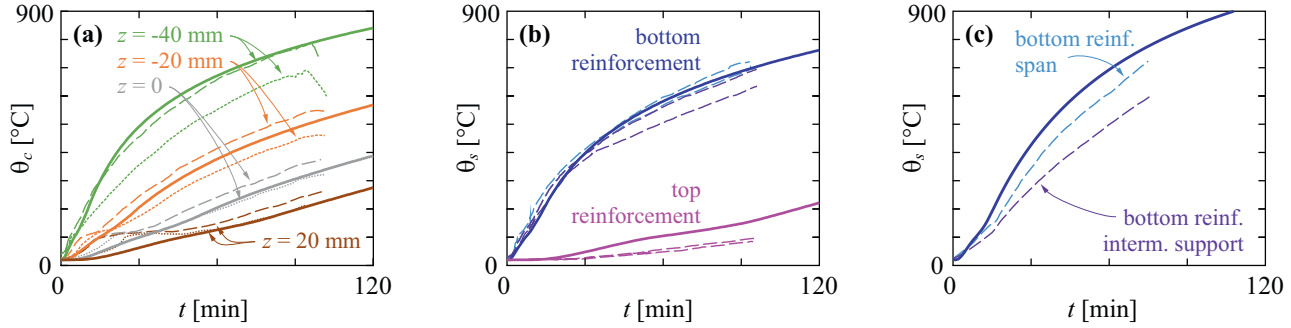

FIGURE 2 Calculated (solid lines) and measured (dashed lines) temperatures as a function of fire duration t, (a) in concrete (θ_c, note that $z = 0$ corresponds to the axis of slab with thickness $h = 100$ mm, exposed to fire at the surface with $z = -50$ mm) and (b) at the reinforcement (θ_s) for Slab 2 (Kordina and Wesche[1]); (c) at the reinforcement (θ_s) for Beam 5 (Wesche[8])

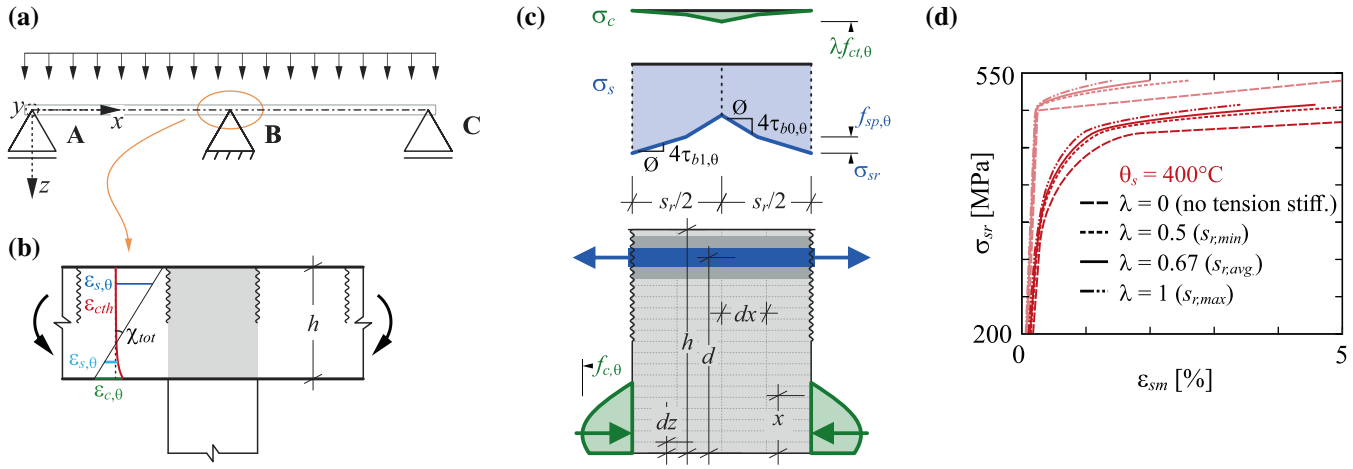

FIGURE 3 Member with tension chord and effect of modeling tension stiffening: (a) exemplary two-span member subjected to bending with coordinate system; (b) cracked region at intermediate support of a member subjected to bending with a possible zone between two cracks in light gray hatch and possible strain distribution in fire conditions; (c) zone between two cracks in detail with compression zone (green) and tensile reinforcement (blue) within a virtual tension chord (dark gray hatch); (d) tension chord behavior of a slab of thickness $h = 250$ mm with $f_{ck} = 20$ MPa, and reinforcing bars ∅12 mm of type B500B spaced at $t = 150$ mm in the tension chord.

reinforcement ratio ρ_t can be defined by equating (i) the maximum steel stress at the crack at the instant of reaching the cracking moment M_{cr} and (ii) the maximum steel stress at cracking of a tension chord:

$$\rho_t = \frac{1}{\frac{M_{cr}(d-x)E_s}{f_{ctm}EI^{II}} + 1 - n}, \tag{2}$$

where d is the effective depth, x is the depth of the compression zone, $n = E_s/E_c$ is the modular ratio = ratio of the Young's moduli of reinforcing steel and concrete at ambient temperature, and EI^{II} is the fully cracked elastic cross-sectional stiffness.[25–27] It is assumed here that Equation (2) also holds if a normal compressive force develops due to restraint during fire exposure, because the cracking moment M_{cr} is generally smaller than the bending moment originating from initial sustained loads in regions where cracking is predominant. This definition of the equivalent geometrical reinforcement ratio in the tension chord is valid with a single reinforcement layer in the tensile zone as common in slabs. Kaufmann et al.[6] proposed an approach to define the equivalent reinforcement ratio with several layers; for a discussion of different approaches see for example,[27]

Using the TCM, the maximum and minimum theoretical crack spacing s_r follow from the condition that the concrete stress at the center between two cracks equals f_{ctm}[4]:

$$s_r = \lambda \frac{\varnothing f_{ctm}(1-\rho_t)}{2\tau_{b0}\rho_t}, \tag{3}$$

where ø is the reinforcing bar diameter. The crack spacing delimits the tension chord element, whose stress and strain distribution can readily be determined by equilibrium, starting at the cracks and using the bond stresses defined above. At the crack, the stress is σ_{sr} and the strain is $\sigma_{sr}/E_{s,\theta}$, corresponding to those of the bare reinforcing bars at equal tensile force. Between the cracks, the concrete carries part of the tensile force and hence, steel stresses and strains are smaller than at the cracks. Figure 3c shows the stress distributions of concrete, σ_c, as well as of reinforcing steel, σ_s, for $\sigma_{sr} > f_{sp,\theta}$ with $\tau_{b0,\theta}$ and $\tau_{b1,\theta}$. As a result of the contribution of the concrete between cracks to the load transfer, the average strains of the tension chord element, ε_{sm}, are smaller than those at the cracks. The resulting difference between the stiffness of the tension chord element and bare reinforcement is known as tension stiffening. For the sake of simplicity, the crack spacing is assumed constant during fire exposure in this study.

Based on the TCM outlined above, a temperature-dependent modified stress–strain relationship accounting for tension stiffening—relating the tensile stress in the reinforcement at the crack σ_{sr} to the average strain ε_{sm} of the tension chord element—can be established by using temperature-dependent material properties for concrete and reinforcement. Figure 3d shows such a relationship based on the stress–strain relationship of bare cold worked reinforcing steel (class N) for $T = 20°C$ and $T = 400°C$ for a slab of thickness $h = 250$ mm with a concrete compressive strength of $f_{ck} = 20$ MPa and reinforcing bars with a diameter of $ø_s = 12$ mm of type B500B, spaced at $t = 150$ mm in the tension chord. It is worth noting that tension stiffening causes higher stiffness and reduced ductility of a tension chord. Both effects are most pronounced with the maximum crack spacing ($\lambda = 1$), corresponding to $s_r \approx 150$ mm in this example, causing a reduction of the ultimate strain of the bare reinforcement

of 0.05 (corresponding to $\lambda = 0$, i.e., no tension stiffening) to merely 0.014 for the tension chord with $\lambda = 1$ at ambient temperature.

3.3 | Mechanical cross-sectional analysis

Figure 4a shows exemplary cross-sectional strain distributions, and Figure 4b shows moment-curvature diagrams, both for a slab of thickness $h = 100$ mm at its ends (Slab 2 of test series by Kordina and Wesche,[1] modeled for siliceous aggregates at $t = 0$, 30, 60 and 90 min). Bending moments and curvatures are positive for the cross-section in the span and negative for the cross-section at the intermediate support; note that the stress-related curvatures $\chi_{tot} - \chi_{th}$ are shown. Such moment-curvature relationships of any cross-section of interest at time t can be determined with a cross-sectional analysis considering (i) the thermal field at time t, (ii) the static boundary conditions (e.g., restraining normal force), (iii) the temperature-dependent material properties specified by EN 1992-1-2 combined with the further specifications outlined in Section 2 and considering tension stiffening as described in Section 3.2 (note that initially cracked sections are assumed). It should be noted that concrete tensile strength is only used to model tension stiffening, while it is neglected for the cross-sectional analysis otherwise. Hence, the concrete tensile strength influences the cross-sectional stiffness but does not influence the strength.

Figure 4a illustrates the procedure for the cross-sectional analysis to obtain points on the moment-curvature diagrams shown in Figure 4b. Based on the thermal expansion ε_{cth} and ε_{sth} from the heat transfer analysis (solid lines in Figure 4a, note that $\varepsilon_{sth,bot}$ is the thermal expansion of bottom reinforcement), a thermal strain plane with curvature χ_{th} (dashed lines) can be found. The thermal strain plane corresponds to the deformations of the mechanically unloaded cross-section. The initial stress-related strains $\varepsilon_{\sigma 0}$, which are the difference of thermal expansion and thermal strains $\varepsilon(\chi_{th})$, dotted lines, lead to stresses determined using temperature-dependent material properties. They cause neither a normal force nor a bending moment when integrated over the cross-section. As commonly assumed in fire design, the hypothesis of plane sections is applied to total strains ε_{tot}, consisting of stress-related strains ε_σ and thermal strains ε_{th} (see e.g. fib Model Code 2010[3]). Hence, the strains $\varepsilon_{\sigma 0}$ need to be added to the total linear strain distribution with curvature χ_{tot} (black dashed line) when determining stresses. The analysis is carried out by varying the total strains defined by the total mid-plane strain and the curvature χ_{tot}.

For computational reasons, the cross-section of interest is divided into layers in the z-direction (see the coordinates and layer with height dz in Figure 3), essentially corresponding to a one-dimensional meshing of the cross-section. For beams exposed to fire on three sides, temperature variations of the concrete in the y-direction are averaged (the principle of this approach for beams corresponds to the sectional analysis suggested by El-Fitiany and Youssef).[28] This simplification of averaging temperature variations in y-direction seems acceptable, as the cross-sectional response of the approach "Simp. (EN)" corresponds well with the finite element analysis "FE (EN)" in Figure 4: Figure 4c shows several moment-curvature diagrams (note that the total curvatures χ_{tot} are shown) for Beam W-5 determined by (i) employing a cross-sectional finite element analysis[29] (solid lines, denominated with "FE (EN)") directly applying the stress–strain relationship for reinforcing steel from EN 1992-1-2 without strain hardening and tension stiffening (see thin dashed line in Figure 1); (ii) using the simplification of averaged temperatures and also applying the stress–strain relationship for reinforcing steel from EN 1992-1-2 without strain hardening and tension stiffening (bold dashed lines, denominated with "Simp. (EN)"); and—for showing the implications of considering strain hardening, limitations

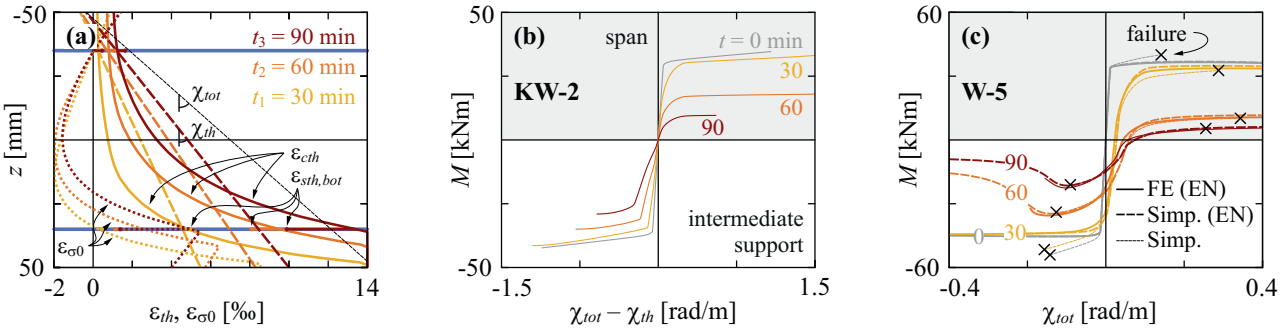

FIGURE 4 Cross-sectional analysis: (a), (b) strain distributions and moment-curvature diagrams of Slab 2 (Kordina and Wesche[1]); (c) moment-curvature diagram of Beam 5 (Wesche[8]), including the comparison of the results obtained with the simplification applied in this study (averaged temperatures in the y-direction) and with a cross-sectional finite element analysis

of the ultimate strain of reinforcement, and tension stiffening on the cross-sectional analysis—(iii) using the simplification of averaged temperatures and applying the tension chord properties defined above (thinner dashed line, denominated with "Simp.").

3.4 | Structural system analysis

Using cross-sectional analyses as outlined above, the curvatures along the member length follow from the bending moment distribution. The deflections of a beam or slab are obtained by twice integrating the total curvatures, including both stress- and temperature-related strains. Deflections compatible with the boundary conditions follow from iterating the bending moment distribution. Accordingly, the behavior of a member subjected to bending can be analyzed for any time during fire exposure by a structural system analysis, ensuring global equilibrium and deformation compatibility.

The rotation demand can be determined by integrating the differences of equal sign between the curvatures at time t and the curvatures at which the reinforcement started yielding. This process implicitly accounts for the varying bending stiffness over the length (x-axis) of the member. The member can be considered to fail once the bending moment exceeds the bending resistance at any point of the member. At this instant, the rotation demand entirely consumes the rotation capacity in the case of statically indeterminate systems. This definition of failure yields conservative fire resistance predictions, as it neglects any residual load-bearing capacity after failure at one section. However, the residual capacity is small for one-way two-span continuous members.[30]

Figure 5a shows the modeled distribution of the total curvatures χ_{tot} along the x-axis of Slab 2 of Kordina and Wesche[1] at $t = 46$ min (instant of failure for siliceous concrete in the numerical simulations) as well as the corresponding calculated displacements for different fire durations. The immediate vicinity of the intermediate support, where the known beneficial effect of a biaxial stress state increases the concrete strength, is hatched in gray in Figure 5a. Thereby, higher curvatures may occur when modeling this region.

While plastic rotations occur at the intermediate support, remarkably large strains may occur in concrete, exceeding what would be expected at ambient temperature. This is illustrated in Figure 5b, which shows the modeled strain evolution of both reinforcement and concrete at the intermediate support during fire exposure. Top reinforcing steel stress-related tensile strains (dark blue) are positive, while concrete (green) and bottom reinforcing steel (light blue, "bottom" abbreviated with "bot") stress-related compressive strains are negative. The maximum calculated stress-related strains of the reinforcing steel $\varepsilon_{s,\theta}$ and the concrete $\varepsilon_{c,\theta}$ are confronted with the maximum reinforcing steel and concrete strains $\varepsilon_{su,\theta}$ $(M_{R,\theta})$ and $\varepsilon_{cu,\theta}$ $(M_{R,\theta})$, respectively, which would be attained under the cross-sectional bending resistance $M_{R,\theta}$ at the considered time step (peak moment determined according to Section 3.3 at the time of interest). For orientation, Figure 5b also shows the thermal expansion of (i) the top and bottom reinforcement ε_{sth} and (ii) the concrete at the exposed surface ε_{cth}, as well as the strains $f_{sp,\theta}/E_{s,\theta}$ associated with the proportional limit.

If parts of the member or adjacent building members are not exposed to fire, the thermal rotations and expansions may be restrained, resulting in bending moments and axial compressive restraint forces, the latter generally acting eccentrically with respect to the section's centroid. In order to study the impact of thermal restraint with the presented model, eccentric spring elements—with constants defining the rotational and axial stiffness—can be introduced to represent adjacent members unaffected by the fire exposure and, thus, not subjected to thermal expansion. Second-order effects were not considered.

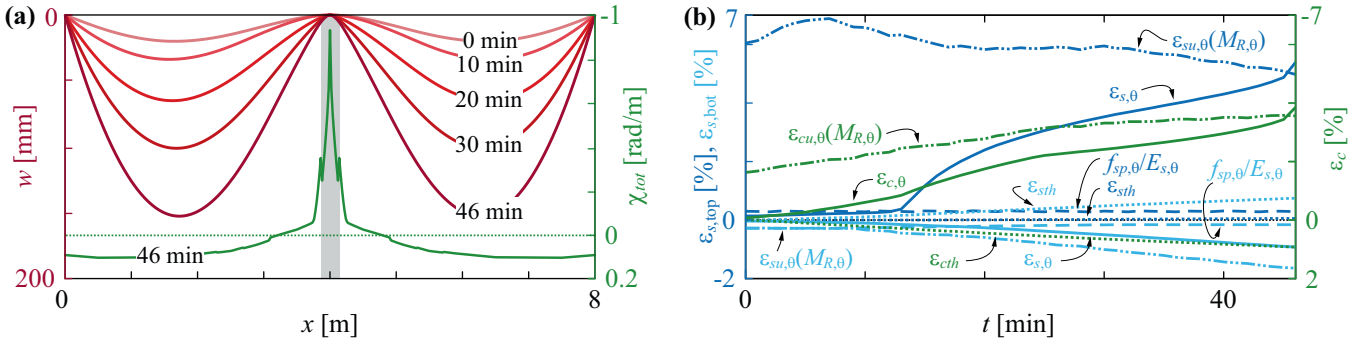

FIGURE 5 Structural system analysis: (a) modeled cross-sectional curvatures and displacements at different time steps until failure (region of intermediate support hatched in gray); (b) modeled evolution of top (dark blue) and bottom (light blue) reinforcement strains and concrete strains (green) at intermediate support during fire exposure. Parameters corresponding to Slab 2 of Kordina and Wesche.[1]

4 | VALIDATION

The model proposed above has been numerically implemented and validated against the results of experimental campaigns.[1,8,9] The campaigns included (i) one-way two-span slabs with free ends, thicknesses of 100, 140, or 150 mm and a total length of 8 m,[1] (ii) T-shaped two-span beams with free ends, varying cross-sections and a total length of 8 m[8] and (iii) rectangular beams with restrained ends, a cross-section of $h \times b = 300$ mm $\times$ 150 mm and a total length of 3 m.[9] A detailed review of the experimental campaigns can be found in Bischof.[30]

The material properties documented in the test reports were used without modification for the predictions presented here. Unless documented, values of $E_s = 205$ GPa and E_{cm} [GPa] $= 10 f_{cm}{}^{1/3}$ were assumed for the Young's modulus of reinforcement and the secant stiffness of concrete, respectively, according to EN 1992-1-1.[16] Wesche[8] did not report the tensile strength, the ultimate strain and the strain at maximum load. For modeling the corresponding beams, the reinforcing steel properties beyond yielding were assumed to $f_{tk} = 1.1 f_{yk}$ for RK steel and $f_{tk} = 1.2 f_{yk}$ for RU steel, while the ultimate strain was assumed as $\varepsilon_{uk} = 0.05$ and $\varepsilon_{uk} = 0.08$, respectively, based on results reported in Kordina and Wesche[1] for the same steel grades.

Where applicable, the curtailment of the bottom reinforcement and the top reinforcement was considered as reported by Wesche,[8] and Kordina and Wesche.[1] The reduction of material properties was applied as described in Section 2, assuming Class N for the reinforcing steel.

4.1 | Modeling

The thermal fields were calculated with transient analyses using a mesh size of 5 mm for the slices in z-direction for slabs, and squares in y- and z-direction for beams, respectively (coordinate system see Figure 3a). For the mechanical analyses, the cross-sections were divided into layers of maximum height of $dz = 5$ mm in the z-direction (see layering in Figure 3c). When using smaller layer heights than the mesh size of the transient analyses, the temperature was linearly interpolated between two values. For the structural system analysis, the length (x-direction) of the studied members was discretised into slices of $dx = 20$ mm (see Figure 3c). A sensitivity analysis for the slice length applied on the continuous slabs and beams showed some inconsistent results for slices larger than a realistic crack spacing (approximately 50...200 mm).

The analyses carried out in this study neglect variations of the thermal field for the cross-sectional moment-curvature relationship along the length of the studied member. Especially, at the intermediate support of the tested members, two- and three-dimensional thermal fields for slabs and beams, respectively, would render more realistic results by capturing the compression zone more accurately. However, extending the analysis in this additional dimension would drastically increase the computational effort.

4.2 | Results

Figures 6–8 compare experimental results (thin dashed lines) to predictions obtained using the model outlined above (solid lines; dark = siliceous aggregates, light = calcareous aggregates).

Figure 6 compares (a) the bending moments M_B at the intermediate support, (b) the maximum deflections w_{Span} in the span, and (c) the reinforcement strains $\varepsilon_{sm,B}$ averaged over 100 mm at the intermediate support in the slabs tested by Kordina and Wesche.[1] For the sake of readability,

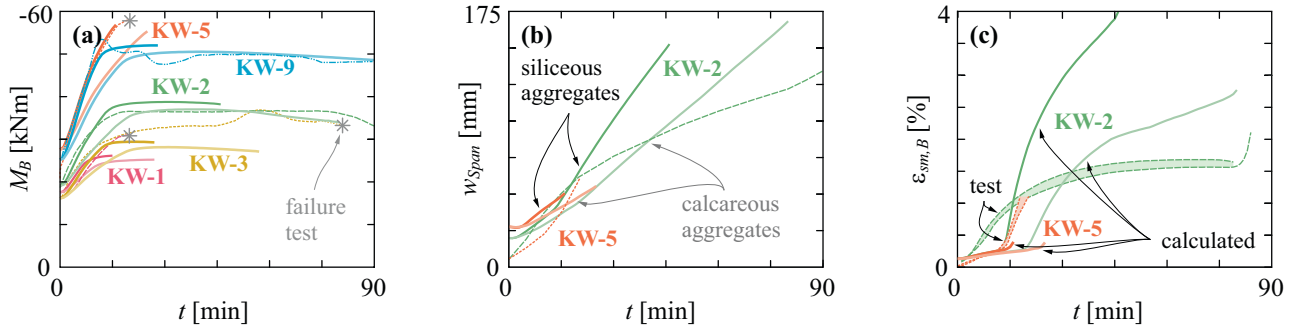

FIGURE 6 Comparison of model predictions (solid lines) and experimental results (dashed lines) for Slabs KW-1, KW-2, KW-3, KW-5, and KW-9 during exposure time t: (a) maximum bending moment at intermediate support (gray asterisks = instant of failure in test); (b) vertical displacement in the span (KW-1: Average of both spans, KW-5: Max. of longer span); (c) stress-related average strains of top reinforcement at intermediate support (two measurements reported per slab).

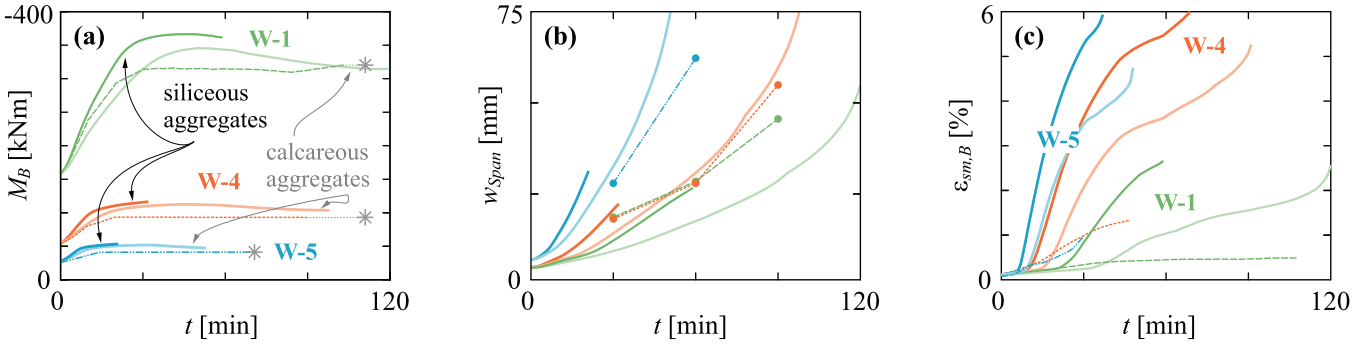

FIGURE 7 Comparison of model predictions (solid lines) and experimental results (dashed lines) for beams W-1, W-4, and W-5 during exposure time t: (a) maximum bending moment at intermediate support (gray asterisks = instant of failure in test); (b) vertical displacements in the span (average of both spans); (c) stress-related average strains of top reinforcement at intermediate support.

Figures 6b,c only show Slabs KW-2 and KW-5; note that in the latter test, the small predicted average strains at the intermediate support (Figure 6c) indicate that the model predicts failure at the end of the top reinforcement. Figure 7 shows the same comparisons for the beams W-1, W-4, and W-5 tested by Wesche.[8] Figure 8 compares (a) the normal force restraint and (b) the maximum deflections w_{Span} in the span of selected beams tested by Albuquerque et al.[9]

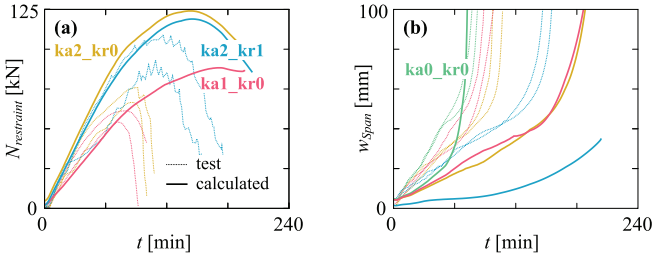

FIGURE 8 Comparison of model predictions (solid lines) and experimental results (dashed lines) for selected beams of Albuquerque et al.[9] during exposure time t: (a) axial restraint forces at the supports; (b) vertical displacements in the span.

4.3 | Discussion

Generally, the model predictions correlate well with the experimental results of the continuous beams and slabs regarding the fire resistance, the evolution of the bending moments at the intermediate support, as well the deflections in the span. The comparison between test results and model predictions reveals a considerable effect of the aggregate type, mainly because of the role played by the thermal expansion.

In the slab KW-3, a slightly larger deviation is observed, underpredicting the bending moment at the intermediate support. However, note that the experimentally observed bending moment at the intermediate support even exceeded the theoretical bending resistance at ambient temperature in this test; nevertheless, Kordina and Wesche[1] did not explain this deviation.

Generally, the predicted average strains at the intermediate support exceed the measured values, more pronouncedly for beams than for slabs. One reason for this overprediction may be that the supporting walls used as intermediate supports generally reduce the bending moment and, consequently, also the tensile strains (e.g., the beam W-1 was supported on a 600 mm thick wall). Furthermore, the model may tend to underestimate the stiffness in the intermediate support region, possibly due to several reasons. First, lower temperatures prevail in this region due to the thermal effect of the supporting wall, which is not accounted for in this article as outlined in Section 4.1. Second, the adopted concrete compressive stress–strain relationship of EN 1992-1-2, while being easy to use and generally acceptably precise in the design phase, cannot model all the different types of concrete used in the presented studies with adequate accuracy. Third and most importantly, not only the stress–strain relationship of concrete in compression but the complete behavior of statically indeterminate members under fire conditions is highly sensitive to the type of aggregates used, as illustrated by Figures 6 and 7, which show predictions for both siliceous and calcareous aggregates. The complexity involved in modeling the compression zone at the intermediate support is crucial for beams, where the compression zone depth tends to absorb a large portion of the member depth, increasing with fire duration.

For the restrained specimens (ka1_kr0, ka2_kr0 and ka2_kr1) from the experimental series of Albuquerque et al.,[9] the comparison of the predicted axial restraint forces and midspan deflections with the measured values reveals that the model overestimates the actual stiffness. However, the predicted and the measured midspan deflections correlate well for the specimen without

restraint (ka0_kr0). A reason for these discrepancies could be second-order effects caused by the experimentally observed horizontal displacements of the restrained specimens of width $b = 150$ mm due to their high geometric slenderness of $\lambda = 91$, not accounted for in the model. While second-order effects are usually decisive in determining the structural behavior in fire conditions, for slabs, their role is definitely less significant. However, Riva and Franssen[31] found a difference of 60 min (240 vs. 180 min) in the computed fire resistance for a beam with height $h = 500$ mm, width $b = 350$ mm and length $l = 6$ m, when comparing the configurations with or without considering second-order effects.

5 | SUMMARY

Calculations to assess the rotation demand and capacity of statically indeterminate reinforced concrete slabs and beams under fire conditions are necessary according to EN 1992-1-2 to allow more than 15% redistribution of bending moments. Nevertheless, EN 1992-1-2 does not indicate how to perform such calculations to prove sufficient rotation capacity. They are not straightforward since (i) rotation demand and rotation capacity cannot be considered separately (as often done at ambient temperature) and (ii) the easy-to-use constitutive model for reinforcing steel from EN 1992-1-2 cannot capture the actual behavior beyond yielding of the tension chord. The realistic modeling of plastic hinges caused by the high restraint moments under fire conditions and their corresponding large rotations is highly relevant for reliably predicting the global response and structural safety of a structure (partially) exposed to fire.

This article presents a comprehensive modeling approach to assess the fire resistance and thereby the rotation capacity of statically indeterminate members subjected to bending under fire conditions. For any fire duration of interest, moment-curvature relationships are used to analyze the structural system subjected to fire and static loads. The moment-curvature behavior of any cross-section of interest at time t is determined with a cross-sectional analysis considering (i) the thermal field, (ii) the boundary conditions (e.g., restraining normal force), and (iii) the material properties. Regarding the latter, the values specified by EN 1992-1-2 are complemented by additional considerations concerning the biaxial compressive strength of concrete, the strain hardening and the limitation of the ultimate strain of the reinforcement. These considerations are particularly relevant because the reinforcement of primary interest at intermediate supports is generally only slightly heated, as it is usually placed at a considerable distance from the member surfaces exposed to fire. Furthermore, tension stiffening with its detrimental effect on the ultimate strain of the tension chord is modeled by extending the established Tension Chord Model to account for fire exposure.

When comparing the results obtained by the model to pertinent experimental results given in the literature, the agreement is good for slabs and beams, however, with a rather considerable uncertainty on the type of concrete aggregate used. It is shown that accurately modeling the region of the intermediate supports, where concrete is heated and under high compression at the same time, is challenging, particularly to obtain reliable predictions of local strains.

AUTHOR CONTRIBUTIONS

Patrick Bischof: Conceptualisation, formal analysis, funding acquisition, investigation, methodology (lead), supervision (lead), writing - original draft (lead). **Urias Morf**: Methodology, software, writing – review, and editing. **Patrick Bamonte**: software, formal analysis, writing – review, and editing. **Walter Kaufmann**: Funding acquisition, writing - original draft, review, and editing, supervision.

ACKNOWLEDGMENT

Open access funding provided by Eidgenossische Technische Hochschule Zurich.

DATA AVAILABILITY STATEMENT

The data that support the findings of this study are openly available in ETH Research Collection at https://www.research-collection.ethz.ch/handle/20.500.11850/533262, reference number DOI: 10.3929/ethz-b-000533262.

ORCID

Patrick Bischof https://orcid.org/0000-0003-3032-5482
Patrick Bamonte https://orcid.org/0000-0002-4967-1089
Walter Kaufmann https://orcid.org/0000-0002-8415-4896

REFERENCES

1. Kordina K, Wesche J. Stahlbeton-Durchlaufkonstruktionen unter Feuerangriff bei Variierung von Stahlart und—güte der Biegezugbewehrung im Stützbereich. Braunschweig: Institut für Baustoffe, Massivbau und Brandschutz, TU Braunschweig; 1979. https://doi.org/10.24355/dbbs.084-201401101434-0
2. EN 1992-1-2. Eurocode 2: Design of concrete structures—Part 1–2: General rules—Structural fire design, Brussels: European Committee for Standardization; 2004.
3. fib. Design. fib Model Code for Concrete Structures. Volume 2013. Berlin: Ernst & Sohn; 2010. p. 190–350. https://doi.org/10.1002/9783433604090.ch7
4. P. Marti, M. Alvarez, W. Kaufmann, and V. Sigrist, 'Tension chord model for structural concrete', Structur Eng Int, vol. 8,

no. 4, pp. 287–298, 1998, https://doi.org/10.2749/101686698780488875.
5. V. Sigrist, Zum Verformungsvermögen von Stahlbetonträgern, Doctoral Thesis, ETH Zurich, 1995. https://doi.org/10.3929/ethz-a-001475252.
6. Kaufmann W, Mata Falcón J, Weber M, Galkovski T, Tran DT, Kabelac J, et al. Compatible stress field design of structural concrete: principles and validation. Zurich, Brno: ETH Zurich, Institute of Structural Engineering (IBK); IDEA StatiCa s.r.o.; 2020. Available from: https://www.research-collection.ethz.ch/handle/20.500.11850/411585.
7. Ehm H, Krampf L, Postel R. Durchlaufende Stahlbetonkonstruktionen unter Brandbeanspruchung. Braunschweig: Institut für Baustoffe, Massivbau und Brandschutz, TU Braunschweig; 1970. https://doi.org/10.24355/dbbs.084-201605301242-0
8. Wesche J. Stahlbetondurchlaufkonstruktionen unter Feuerangriff: Bericht. Braunschweig: Institut für Baustoffe, Massivbau und Brandschutz, TU Braunschweig; 1974. https://doi.org/10.24355/dbbs.084-201906241320-0
9. Albuquerque GL, Silva AB, Rodrigues JPC, Silva VP. Behavior of thermally restrained RC beams in case of fire. Eng Struct. 2018; 174:407–17. https://doi.org/10.1016/j.engstruct.2018.07.075
10. Bischof P, Morf U, Kaufmann W. Assessment of parameters influencing the behaviour of restrained reinforced concrete slabs and beams under fire conditions. *fib Structural Concrete*; 2022:1–14. https://doi.org/10.1002/suco.202200318
11. Lo Monte F, Kalaba N, Bamonte P. On the extension of a plastic-damage model to high temperature and fire. Presented at the IFireSS 2017—2nd International Fire Safety Symposium. Naples, Italy: Doppiavoce; 2017.
12. Elghazouli AY, Cashell KA, Izzuddin BA. Experimental evaluation of the mechanical properties of steel reinforcement at elevated temperature. Fire Saf J. 2009;44(6):909–19. https://doi.org/10.1016/j.firesaf.2009.05.004
13. Cadoni E, Dotta M, Forni D. Tensile behaviour of reinforcing steels at high strain rate and high temperature. Key Eng Mater. 2016;711:791–8. https://doi.org/10.4028/www.scientific.net/KEM.711.791
14. Shakya AM, Kodur VKR. Effect of temperature on the mechanical properties of low relaxation seven-wire prestressing strand. Construct Build Mater. 2016;124:74–84. https://doi.org/10.1016/j.conbuildmat.2016.07.080
15. Quiel SE, Irwin CH, Naito CJ, Vermaak N. Mechanical characterization of Normal and high-strength steel bars in reinforced concrete members under fire. J Structur Eng. 2020;146(7):04020110. https://doi.org/10.1061/(ASCE)ST.1943-541X.0002644
16. EN 1992-1-1. Eurocode 2: Design of concrete structures—Part 1–1: General rules and rules for buildings, Brussels: European Committee for Standardization; 2004.
17. Bošnjak J, Sharma A, Öttl C. Modified beam-end test setup to study the bond behavior of reinforcement in concrete after fire. Mater Struct. 2018;51(1):13. https://doi.org/10.1617/s11527-018-1138-7
18. Dwaikat MB, Kodur VKR. A numerical approach for modeling the fire induced restraint effects in reinforced concrete beams. Fire Saf J. 2008;43(4):291–307. https://doi.org/10.1016/j.firesaf.2007.08.003
19. Zehfuß J, Robert F, Spille J, Razafinjato RN. Evaluation of Eurocode 2 approaches for thermal conductivity of concrete in case of fire. Civil Eng Design. 2020;2(3):58–71. https://doi.org/10.1002/cend.202000001
20. Beeby AW. The prediction of crack widths in hardened concrete. Structur Eng. 1979;57A(1):9–17.
21. Meier HH. Berücksichtigung des wirklichkeitsnahen Werkstoffverhaltens beim Standsicherheitsnachweis turmartiger Stahlbetonbauwerke', Doctoral Thesis. Stuttgart: Institut für Massivbau der Universität Stuttgart; 1983.
22. Heinzmann D. Rissbreitenbeschränkung und Mindestbewehrung. Zürich: Aktuelle Fragen und Entwicklungen im Brückenbau; 2016.
23. Barre F, Bisch P, Danièle C, Cortade J, Jean-François C, Jean-Philippe D, et al. Cracking of ties. Control of cracking in reinforced concrete structures. Hoboken: John Wiley & Sons, Ltd; 2016. p. 47–57. https://doi.org/10.1002/9781119347088.ch3
24. H. Seelhofer, 'Ebener Spannungszustand im Betonbau: Grundlagen und Anwendungen', Doctoral Thesis, ETH Zurich, 2009. https://doi.org/10.3929/ethz-a-005901914.
25. Marti P. Structural Concrete. ETH Zürich: Institute of Structural Engineering; 2007.
26. C. Burns, Serviceability analysis of reinforced concrete based in the tension chord model, Doctoral Thesis, ETH Zurich, 2011. https://doi.org/10.3929/ethz-a-007179384.
27. Galkovski T, Mata-Falcón J, Kaufmann W. Effective reinforcement ratio of RC beams: validation of modelling assumptions with high-resolution strain data. Structur Concr. 2022;3:1353–69. https://doi.org/10.1002/suco.202100739
28. S. F. El-Fitiany and M. A. Youssef, 'Simplified method to analyze continuous reinforced concrete beams during fire exposure', SJ, vol. 111, no. 1, pp. 145–156, 2014, https://doi.org/10.14359/51686544.
29. Bamonte P. A reappraisal of the nominal curvature method in the fire design of reinforced concrete columns. J Fire Sci. 2020; 38(2):1–16. https://doi.org/10.1177/0734904119895436
30. P. Bischof, 'Review of restrained reinforced concrete slabs and beams under fire conditions', *in preparation*.
31. Riva P, Franssen JM. Non-linear and plastic analysis of RC beams subjected to fire. Structur Concr. 2008;9(1):31–43. https://doi.org/10.1680/stco.2008.9.1.31

AUTHOR BIOGRAPHIES

Patrick Bischof Institute of Structural Engineering (IBK) ETH Zurich Zurich, Switzerland

Urias Morf Institute of Structural Engineering (IBK) ETH Zurich Zurich, Switzerland

Patrick Bamonte Department of Civil and Environmental Engineering (DICA) Politecnico di Milano Milan, Italy

Walter Kaufmann Institute of Structural Engineering (IBK) ETH Zurich Zurich, Switzerland

How to cite this article: Bischof P, Morf U, Bamonte P, Kaufmann W. Modeling statically indeterminate reinforced concrete slabs and beams under fire conditions. Structural Concrete. 2022. https://doi.org/10.1002/suco.202200319